



HAL
open science

A doubly reduced approximation for the solution to PDE's based on a domain truncation and a reduced basis method: Application to Navier-Stokes equations

Elise Grosjean, Yvon Maday

► To cite this version:

Elise Grosjean, Yvon Maday. A doubly reduced approximation for the solution to PDE's based on a domain truncation and a reduced basis method: Application to Navier-Stokes equations. 2023. hal-03588508v3

HAL Id: hal-03588508

<https://hal.science/hal-03588508v3>

Preprint submitted on 22 Mar 2023

HAL is a multi-disciplinary open access archive for the deposit and dissemination of scientific research documents, whether they are published or not. The documents may come from teaching and research institutions in France or abroad, or from public or private research centers.

L'archive ouverte pluridisciplinaire **HAL**, est destinée au dépôt et à la diffusion de documents scientifiques de niveau recherche, publiés ou non, émanant des établissements d'enseignement et de recherche français ou étrangers, des laboratoires publics ou privés.

A doubly reduced approximation for the solution to PDE's based on a domain truncation and a reduced basis method: Application to Navier-Stokes equations

Elise Grosjean*

Yvon Maday[†]

March 22, 2023

Abstract

This paper focuses on the non-intrusive reduced basis (NIRB) method called the *two grids method*. It is used for the simulation of parametric partial differential equations to reduce the associated computational costs of a High-Fidelity code when such problems must be solved for a large number of parameter values or provide a solution in “real time”.

As other reduced basis approaches, the “offline step” relies on the High-Fidelity method with a fine enough grid. On the contrary, the non-intrusiveness of the original *two grids method* is based on the use, in the “online step”, of the same method with a much coarser grid, which considerably reduces the cost of this step.

We extend here this idea by further reducing the “online step” and further simplify the High-Fidelity method. As an example of application we consider a classical fluid problem, the 2D Backward Facing Step (BFS). We simplify the model by i) truncating the outflow part of the channel at extreme and ii) using a coarse uniform mesh instead of refining it at the re-entrant corner, both choices that contradict what is required to get a high fidelity representation of the flow. To accomplish this, we create two reduced bases and a deterministic process that allows us to pass from one to the other.

Several numerical simulations illustrate the ability of this new approach.

1 Introduction

Reduced Basis Methods (RBM) are widely used to approximate the solutions of parameter-dependent problems for a large number of parameter values within a parameter space. The latter enables the definition of the solutions manifold, which contains the solutions for all parameters within the parameter space. RBM are based on the assumption that the solutions manifold has a small Kolmogorov N -width [32]. In other words, they take advantage of the fact that the solutions for a wide range of parameters share similar physical behaviors, so that only a few well-chosen solutions are sufficient to approximate well any element of the solution manifold by linear combination. These carefully selected elements are known as *snapshots*. They are exploited to construct a *reduced space* that must be close to the solution manifold. Then for a new parameter, the associated solution may be approached very quickly but accurately by projecting it onto this space.

Several RBM exist [38, 27, 30, 2, 40, 8]. They usually take advantage of a procedure decomposition into two steps, one “offline” and one “online”. The snapshots are computed using a High-Fidelity (HF) code during the offline portion. Any classical method, such as the Finite Element Method (FEM) or Finite Volume schemes (FVM), may be used in this code. Then, during the online part, a reduced problem is solved.

The ability to modify the HF code is frequently required for an efficient implementation of these methods. Yet, if the code has been purchased, as it is frequently the case in industry, this may be impossible. This is why we focus on the two grids method, which is a Non-Intrusive Reduced Basis (NIRB) algorithm [11, 9, 12, 22] (see also different NIRB methods from the two-grid algorithm [8, 18, 2]). Indeed, it does not require any change to the HF code and instead employs it solely as a “black-box” solver. We refer to [24, 36] for another approach of non-intrusiveness based on the learning of reduced operators through neural network framework.

*RPTU Kaiserslautern-Landau, Gottlieb-Daimler-Straße 47 Kaiserslautern, Germany (grosjean@mathematik.uni-kl.de).

[†]Sorbonne Université and Université de Paris, CNRS, Laboratoire Jacques-Louis Lions (LJLL), 4 Place Jussieu (yvon.maday@sorbonne-universite.fr) & Institut Universitaire de France

1.1 Reminders on the classical NIRB two-grid method

Let Ω be a bounded domain in \mathbb{R}^d , with $d \leq 3$ and a smooth enough boundary $\partial\Omega$, and consider a parametric problem \mathcal{P} on Ω . Here, we consider time-independent problems (see [23] for parabolic equations). Let μ represent a parameter of \mathcal{P} chosen in a given set \mathcal{G} and $\mathbf{u}(\mu)$ the associated solution. The manifold of all solutions is defined as

$$\mathcal{S} = \{\mathbf{u}(\mu), \mu \in \mathcal{G}\}.$$

Thanks to numerous HF solutions of \mathcal{P} already computed for various parameter values, we want to approximate quickly the solution for a new parameter $\tilde{\mu} \in \mathcal{G}$.

In what follows, we consider a FEM HF code to approximate any solution in \mathcal{S} .

The particularity of the two-grid method is to be based on two FEM meshes:

- one fine mesh \mathcal{T}_h , with which the HF snapshots during the offline part are generated,
- one coarse mesh \mathcal{T}_H , where the problem solution is computed online with the new parameter $\tilde{\mu} \in \mathcal{G}$.

The latter is what makes the method so efficient. Because it is based on a coarse FEM approximation, the NIRB solution computation for the new parameter $\tilde{\mu}$ is very inexpensive and thus allows to recover the full efficiency of the classical RBM. The approximation is then improved in a very brief runtime by projection and rectification onto the reduced space using a Reduced Basis (RB) of this space created independently during the offline part. The FEM HF solutions calculated on \mathcal{T}_h are denoted by $\mathbf{u}_h(\mu)$, while the FEM solution approximations computed on the coarse mesh \mathcal{T}_H are denoted by $\mathbf{u}_H(\mu)$.

The offline-online decomposition of this method is as follows:

- **“Offline step”**

The offline part can be thought as a learning procedure and allows us to construct the reduced space. All expensive parts of the algorithm are performed during this step.

1. We begin by defining a large enough training set of parameters

$$\mathcal{G}_{train} := \bigcup_{i \in \{1, \dots, N_{train}\}} \mu_i.$$

Then, in order to generate the reduced space, we use a greedy technique that selects appropriate parameters $(\mu_i)_{i=1, \dots, N}$ within \mathcal{G}_{train} . As it is standard in RBM framework, at each greedy iteration, the new RB parameter in \mathcal{G}_{train} is chosen such that its associated solution is the poorest approached by the former basis space. The algorithm 1 describes this greedy procedure. Note that another way for generating the RB is to use the Snapshots POD [38, 42, 40, 34].

In algorithm 1, inexpensive a-posteriori error estimates may replace $\left\| \mathbf{u}_h(\mu) - P^{k-1}(\mathbf{u}_h(\mu)) \right\|_{L^2}$ and reduce its computational time [5, 35, 6, 44, 37].

In practice, the greedy algorithm is halted with a stopping criterion such as an error threshold or a maximum number of basis functions that can be generated. At the end of the algorithm (as in algorithm 1 above), the space $X_h^N := \text{Span}\{\Phi_1^h, \dots, \Phi_N^h\}$ is thus provided with an orthonormal basis.

2. Then, in order to stabilize the approximation we can propose, as an option, a new basis set: we solve the following eigenvalue problem:

$$\begin{aligned} &\text{Find } (\Psi^h, \lambda) \in (X_h^N, \mathbb{R}) \text{ such that:} \\ &\forall v \in X_h^N, \int_{\Omega} \nabla \Psi^h \cdot \nabla v \, d\mathbf{x} = \lambda \int_{\Omega} \Psi^h \cdot v \, d\mathbf{x}, \end{aligned} \quad (1)$$

We get an increasing sequence of eigenvalues λ_i , and orthogonal eigenfunctions $(\Phi_i^h)_{i=1, \dots, N}$, orthogonalized both in $L^2(\Omega)$ and $H^1(\Omega)$ that we choose to normalize in $L^2(\Omega)$. It is worth noting that the Gram-Schmidt method of the traditional greedy algorithm 1 yields only an $L^2(\Omega)$ -orthonormalized RB. As a result, as detailed in [21], it stabilizes the NIRB approximation with respect to N . For the sake of simplicity, we continue to name Φ this improved reduce basis i.e. we set $\Phi_k^h = \Psi_k^h$.

- 1: **Input:** tol , $\{\mathbf{u}_h(\mu_1), \dots, \mathbf{u}_h(\mu_{N_{train}})\}$ with $\mu_i \in \mathcal{G}_{train}$.
- 2: **Output:** Reduced basis $\{\Phi_1^h, \dots, \Phi_N^h\}$.
- 3: Choose $\mu_1 = \underset{\mu \in \mathcal{G}_{train}}{\operatorname{argmax}} \|\mathbf{u}_h(\mu)\|_{L^2(\Omega)}$,
- 4: Set $\Phi_1^h = \frac{\mathbf{u}_h(\mu_1)}{\|\mathbf{u}_h(\mu_1)\|_{L^2(\Omega)}}$.
- 5: Set $\mathcal{G}_1 = \{\mu_1\}$ and $X_h^1 = \operatorname{span}\{\Phi_1^h\}$.
- 6: **for** $k = 2$ to N **do**
- 7: $\mu_k = \underset{\mu \in \mathcal{G}_{train} \setminus \mathcal{G}_{k-1}}{\operatorname{argmax}} \|\mathbf{u}_h(\mu) - P^{k-1}(\mathbf{u}_h(\mu))\|_{L^2(\Omega)}$,
- 8: with $P^{k-1}(\mathbf{u}_h(\mu)) := \sum_{i=1}^{k-1} (\mathbf{u}_h(\mu), \Phi_i^h) \Phi_i^h$.
- 9: Compute $\tilde{\Phi}_k^h = \mathbf{u}_h(\mu_k) - P^{k-1}(\mathbf{u}_h(\mu_k))$ and set $\Phi_k^h = \frac{\tilde{\Phi}_k^h}{\|\tilde{\Phi}_k^h\|_{L^2(\Omega)}}$.
- 10: Set $\mathcal{G}_k = \mathcal{G}_{k-1} \cup \{\mu_k\}$ and $X_h^k = X_h^{k-1} \oplus \operatorname{span}\{\Phi_k^h\}$.
- 11: Stop when $\|\mathbf{u}_h(\mu) - P^{k-1}(\mathbf{u}_h(\mu))\|_{L^2(\Omega)} \leq tol, \forall \mu \in \mathcal{G}_{train}$.
- 12: **end for**

Algorithm 1: Greedy algorithm

3. Finally, as a further option, in order to improve the NIRB two-grid approximation, we can now employ a post-treatment step. We remark that the projection of the coarse FEM solution onto X_h^N differs from the projection of the HF snapshot $\mathbf{u}_h(\mu_k)$ computed in the offline stage for any parameter of the RB space $\mu_k, k = 1, \dots, N$. Thus, we resort to the ‘‘rectification post-processing’’, as introduced in [11], to improve the NIRB accuracy.

To this purpose, we create a rectification matrix denoted \mathbf{R} . This matrix is constructed from the HF snapshots $\{\mathbf{u}_h(\mu_k)\}_{k=1, \dots, N}$ and coarse snapshots generated on \mathcal{T}_H with the same parameters μ_k as for the fine ones.

For all $i = 1, \dots, N$, and for all $\mu_k \in \mathcal{G}_{train}$, we define the *coarse coefficients* as

$$A_{k,i} = \int_{\Omega} \mathbf{u}_H(\mu_k) \cdot \Phi_i^h \, d\mathbf{x}, \quad (2)$$

and the *fine coefficients* as

$$B_{k,i} = \int_{\Omega} \mathbf{u}_h(\mu_k) \cdot \Phi_i^h \, d\mathbf{x}. \quad (3)$$

Then, we compute the vectors

$$\mathbf{R}_i = (\mathbf{A}^T \mathbf{A} + \delta \mathbf{I}_N)^{-1} \mathbf{A}^T \mathbf{B}_i, \quad i = 1, \dots, N, \quad (4)$$

where \mathbf{I}_N refers to the identity matrix and δ is a regularization parameter.

- ‘‘Online step’’

The online part of the algorithm is much faster than a fine HF FEM evaluation.

1. We solve the problem \mathcal{P} on the coarse mesh \mathcal{T}_H with the new parameter $\tilde{\mu} \in \mathcal{G}$ we are interested in.
2. Finally, the approximation used in the two-grid method (with the rectification post-treatment step) is

$$\mathbf{R}[u_{Hh}^N](\tilde{\mu}) := \sum_{i,j=1}^N R_{ij} (\mathbf{u}_H(\tilde{\mu}), \Phi_j^h) \Phi_i^h, \quad (5)$$

where $(\mathbf{R})_{ij} = R_{ij}$ is the rectification matrix, given by (4).

1.2 Main contributions

The original version of the NIRB method still suffers from the cost of the online step which is certainly reduced by the use of the coarse grid but may still represent a high cost.

To summarize our contributions, we propose and implement two new ideas to reduce the costs of the algorithm's online component.

- The first one relies on the truncation of the coarse computational domain and the use of a second reduced basis set. The method is described in section 2 and illustrated in 2.3 with several numerical results on a model problem which is a classical fluid problem that of the Backward-Facing Step, described in section 2.2.
- Then, we propose a new strategy for improving NIRB approximation accuracy when dealing with domain singularities without increasing online stage computational times. This is the purpose of the section 3.1 where we present new results on the BFS problem.

2 Domain truncation

The underlying idea is to consider that, for a parameterized PDE, posed on a domain Ω , some main characteristics of its solution depend little on the exact shape of the domain. Some specificities of the domain must of course be respected (e.g. distinctive aspects of the boundary, corners, edges, or aspect ratios) but one can think of reducing the domain (allowing to reduce the number of degrees of freedom of the discretization). If, having thus reduced the size of the domain, the two solutions for the same parameters of the PDE can be associated in a bijective way, one can approach the first one (called virtual solution on the reduced domain) to intuit the second one (called real solution on the initial domain). We propose to learn how to go from the virtual solution to the real solution. To allow this learning, we will look at the solutions under the contracted form of their writing in reduced space... hence the appearance of a second reduced basis associated to the solutions on the reduced domain.

2.1 Description of the Non-Intrusive Reduced Basis tool with domain truncations

Let us consider a "truth" domain $\Omega \in \mathbb{R}^d$ with $d \leq 3$ employed for the simulation, adapted to the parameterized problem.

We then introduce $\omega \subset \Omega$, a truncation of Ω , reduced with fictitious boundaries. The NIRB method with the domain truncation involves two partitioned meshes:

- the classical fine mesh \mathcal{T}_h on Ω ,
- and one coarse mesh \mathcal{T}_H on ω ,

where h and H are the respective sizes of the meshes and $h \ll H$. The size h (resp. H) is defined as

$$h = \max_{K \in \mathcal{M}_h} h_K \text{ (resp. } H = \max_{K \in \mathcal{M}_H} H_K), \quad (6)$$

where the diameter h_K (or H_K) of any element K in a mesh is equal to $\sup_{x,y \in K} |x - y|$.

Let $\tilde{\mu} \in \mathcal{G}$ be the new parameter we are interested in.

- The "offline" part of the algorithm is costly in time but only done once.
 1. Point 1 of the classical NIRB two-grid method remains the same (see section 1.1 and algorithm 1). We generate the RB $(\Phi_i^h)_{i=1,\dots,N_1}$ from suitable parameters $(\mu_1, \dots, \mu_{N_1}) \in \mathcal{G}_{train}^{N_1}$ and the reduced space $X_h^{N_1} = \text{span}\{\Phi_1^h, \dots, \Phi_{N_1}^h\}$. Taking inspiration from [10], where two POD RB are used to reduce the condition number of the rectification matrix (4), we create another RB. We generate this new RB denoted $(\Phi_i^H)_{i=1,\dots,N_2}$ from several parameters $(\mu'_1, \dots, \mu'_{N_2}) \in \mathcal{G}_{train}^{N_2}$. It is constructed on the coarse mesh \mathcal{T}_H by repeating point 1 again but with the coarse snapshots instead of the fine ones. We denote by $X_H^{N_2} = \text{span}\{\Phi_1^H, \dots, \Phi_{N_2}^H\}$ the

new reduced space approaching the manifold of the coarse solutions on the truncated domain $\omega \subset \Omega$.

The coarse solutions are represented by the coarse RB well (respectively the fine solutions with the fine RB). The number of necessary basis functions N_1 and N_2 may be chosen thanks to a small a priori given threshold (tol in algorithm 1). Note that point 2 of the classical NIRB two-grid method may be applied for both RB to obtain H^1 orthogonalized functions.

2. We deal with two kinds of coefficients:

- the fine ones, which correspond to the $L^2(\Omega)$ -inner product of the fine snapshots with the fine RB on the whole domain Ω ,
- and the coarse coefficients, which are the $L^2(\omega)$ -inner product of the coarse snapshots with the coarse RB on the subdomain ω .

In analogy with the two-grid rectification post-treatment, we introduce a rectification matrix \mathbf{T} which allows us to go from the new coarse coefficients to the fine ones.

For all $i = 1, \dots, N_2$, and for all $\mu_k \in \mathcal{G}_{train}$, we define these new *coarse coefficients* as

$$C_{k,i} = \int_{\omega} \mathbf{u}_H(\mu_k) \cdot \Phi_i^H \, d\mathbf{x}, \quad (7)$$

and the *fine coefficients* are defined by (3) with $N = N_1$.

The aim of this processing stage is to seek \mathbf{T}_i minimizing $\|\mathbf{C}\mathbf{T}_i - \mathbf{B}_i\|^2$. The solution of this minimization problem with a regularization parameter [41] are the rectification vectors:

$$\mathbf{T}_i = (\mathbf{C}^T \mathbf{C} + \lambda \mathbf{I}_{N_2})^{-1} \mathbf{C}^T \mathbf{B}_i, \quad \forall i = 1, \dots, N_2, \quad (8)$$

where λ is the regularization parameter.

- The “**online**” step is then performed on the coarse mesh \mathcal{T}_H , which is much less expensive than an HF computation. The online part is even less computationally expensive than the usual NIRB online algorithm because the coarse mesh is computed on $\omega \subset \Omega$ and no interpolation is required to compute the coarse coefficients (7). The coarse solution coefficient is then corrected using the matrix \mathbf{T} before being projected onto the fine RB.

Thus, it consists in:

1. solving the parameterized problem with the FEM solver on the coarse mesh \mathcal{T}_H for the new parameter $\tilde{\mu} \in \mathcal{G}$.
2. setting the new NIRB approximation as

$$\mathbf{T}[\mathbf{u}_{Hh}^N](\mu) = \sum_{i=1}^{N_1} \sum_{j=1}^{N_2} \mathbf{T}_{ij} (\mathbf{u}_H(\tilde{\mu}), \Phi_j^H)_{L^2(\omega)} \Phi_i^h. \quad (9)$$

2.2 A problem model: the 2D Backward Facing Step (BFS)

We consider the 2D Backward Facing Step (BFS) with steady Navier-Stokes. It simulates a fluid flowing through a channel with a descending stair and constitutes an important test for numerical simulations in fluid mechanics. It has been widely studied [16, 28, 15, 33, 19].

The flow is laminar and incompressible in our case, and the channel domain Ω_{∞} is assumed to be infinite, with upper and lower walls. To cope with this infinite domain in simulations, we introduce artificial boundaries and use Neumann boundary conditions on the channel’s exit border and Dirichlet conditions at the entrance. Thus let us consider as our spatial domain $\Omega \subset \Omega_{\infty}$, the channel used for the simulations. The length of the channel to simulate the flow is chosen such that we observe

- a Poiseuille flow and a maximum velocity at the upstream of the channel,
- a vortex at the concave corner behind the step,
- and a Poiseuille flow at the backstream of the channel.

The artificial boundaries must not be too close, so as to not interfere with the modeling, and not too far, to avoid too expensive calculations. The conditions on these artificial boundaries result from the modeling phase.

The channel Ω , which is already a truncation of the infinite channel Ω_∞ , is described by $\Omega = (0, L_1] \times (H_1 - H_0, H_1) \cup (L_1, L) \times (0, H_1)$ as shown in Figure 1.

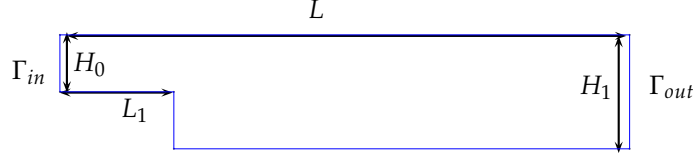


Figure 1: The flow channel

\mathbb{R}^2

Therefore, we consider the following parameter-dependent problem \mathcal{P} as our model problem:

Find the velocity of the fluid $\mathbf{u} \in H^1(\Omega)^2$ and the pressure $p \in L^2(\Omega)$, solutions of the steady Navier-Stokes equation

$$\left\{ \begin{array}{l} \mathbf{u} \cdot \nabla \mathbf{u} - \nu \Delta \mathbf{u} + \nabla p = 0 \text{ on } \Omega, \\ \nabla \cdot \mathbf{u} = 0 \text{ on } \Omega, \\ \mathbf{u}(\mathbf{x}) = \begin{bmatrix} \frac{4}{H_0^2} (H_1 - x_2) (x_2 - H_1 + H_0) \\ 0 \end{bmatrix} \text{ on } \Gamma_{in}, \\ \nu \partial_{\mathbf{n}} \mathbf{u}|_{\Gamma} - p \mathbf{n} = 0 \text{ on } \Gamma_{out}, \\ \mathbf{u}(\mathbf{x}) = 0, \text{ on } \partial\Omega \setminus (\Gamma_{out} \cup \Gamma_{in}), \end{array} \right. \quad (10)$$

where $\mathbf{x} = (x_1, x_2) \in \Omega$, $\mathbf{u} = (u_1, u_2)$, and $\nu = \frac{1}{Re}$, Re being the *Reynolds number*. The solution of this problem is uniquely defined by the data $[\nu, H_0, L_1, H_1, L]$. We consider

$$\mu := Re \in \mathcal{G} = [30, 300]$$

as the problem variable parameter. Note that, for $Re > 300$, there is no stable steady solution with the geometric data we consider $H_0 = 0.5$, $H_1 = 1$, and $L_1 = 1$.

2.3 Numerical results on the model problem

We have carried out numerical simulations for equations (10) in FreeFem++ (version 4.9) [25] with the Newton algorithm for the numerical treatment of the nonlinear term, and classical Taylor-Hood finite elements $\mathbb{P}_2 - \mathbb{P}_1$. The fine mesh size is equal to 0.03, and the coarse one to 0.21. We have used a finer mesh with a size equal to 0.016 as a surrogate for the solutions of reference in order to compute the errors accurately.

For the fine mesh \mathcal{T}_h , we have set the length of the channel (which does not change) to $L = 5$. Thus, in what follows, L refers to the length of the subdomain ω . We recall that the Reynolds number $Re \in \mathcal{G} = [30, 300]$ is the problem parameter, and the domain Ω is truncated according to $L \in [1, 5]$ (remember that $L \leq L_1 = 1$). The size of the coarse mesh $H < 1$ is such that $H^2 \simeq h$. For instance, Figure 2 represents the two partitioned meshes with $L = 3$ for the length of the coarse mesh.

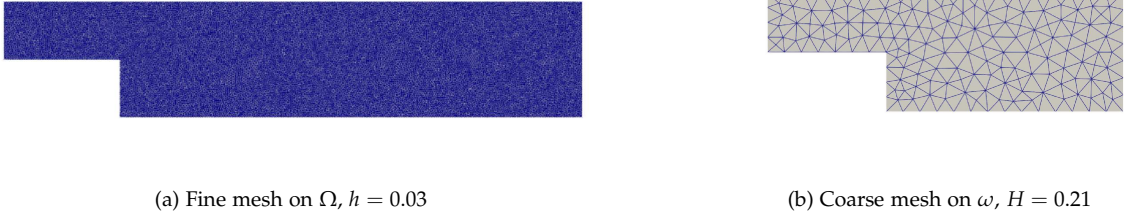


Figure 2: Fine and coarse meshes

When the Reynolds number increases, the recirculation after the step is expanded, as shown in Figure 3. Thus, we also consider two subgroups of \mathcal{G} :

$$\mathcal{G}_1 = [30, 150[\text{ with } \mathcal{G}_{1,train} = \{30 + 15i, \quad i = 0, \dots, 7\}, \quad (11)$$

$$\mathcal{G}_2 = [150, 300] \text{ with } \mathcal{G}_{2,train} = \{30 + 15i, \quad i = 8, \dots, 18\}, \quad (12)$$

$$\text{and } \mathcal{G} = [30, 300], \quad \mathcal{G}_{train} = \mathcal{G}_{1,train} \cup \mathcal{G}_{2,train}$$

from which we extract, with three greedy methods, three reduced bases of size $N_1 = 1, \dots, 8$, $N_2 = 1, \dots, 11$, and $N_3 = 1, \dots, 19$.

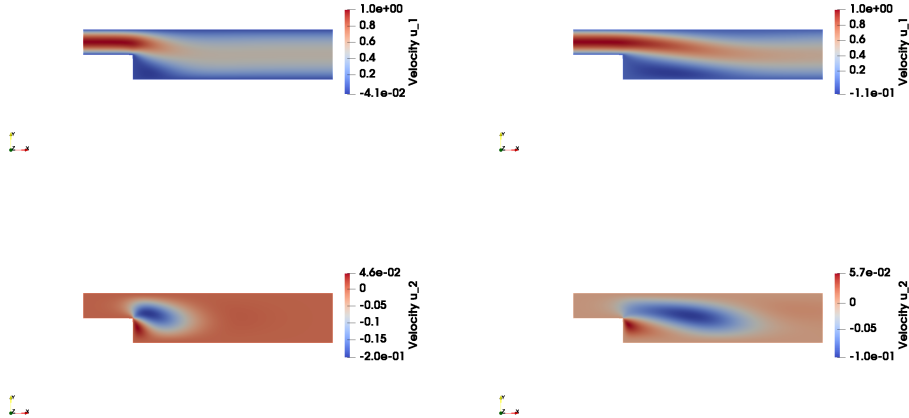


Figure 3: Velocities (u_1 and u_2) for Reynolds=52 (left) and Reynolds=233 (right)

Then we have generated the FEM solutions of two new parameters in \mathcal{G} : $Re = 52$ and $Re = 233$. The coarse solutions for $Re = 52$ on the truncated subdomains with $L = 1.2$ and $L = 3$ are presented in Figure 4.

We have tried several values for the parameter $L \in [1, 5]$. In the following figures, we present the results of the new NIRB algorithm in order to analyze its limits and observe the effects of domain truncations on the phenomena. Our results display *the H^1 relative error*

- between the \mathbf{u}_{ref} and the coarse and fine HF solutions,
- obtained by the classical NIRB algorithm of section 1.1, with the rectification postprocessing step (4), as illustrated in Figure 5. With the classical NIRB (5), the error is given by

$$\frac{\left\| \mathbf{u}_{ref}(\tilde{\mu}) - \mathbf{u}_{Hh}^N(\tilde{\mu}) \right\|_{H^1(\Omega)}}{\left\| \mathbf{u}_{ref}(\tilde{\mu}) \right\|_{H^1(\Omega)}}.$$

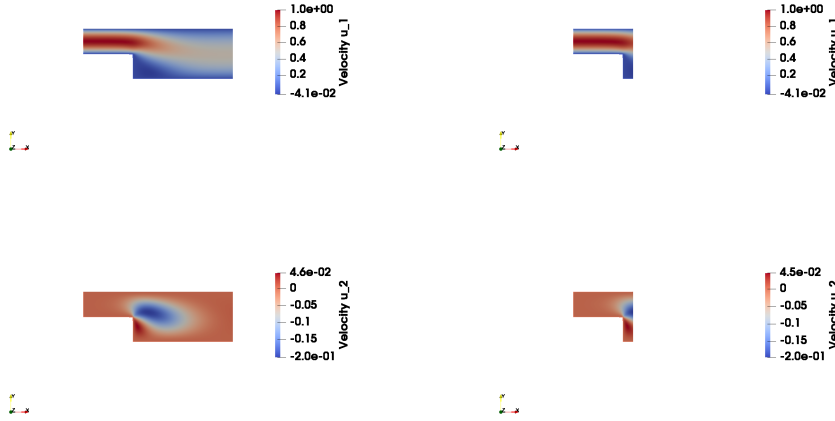


Figure 4: Coarse velocities u_1 (up), u_2 (bottom), $Re = 52$ on the truncated domain with $L = 3$ (left), and with $L = 1.2$ (right)

We find that the error between $\mathbf{u}_{ref}(\tilde{\mu})$ and $\mathbf{u}_h(\tilde{\mu})$ can be recovered if the new Reynolds parameter belongs to the parameters group used for the RB generation. It requires 4 modes for an RB generated from the group \mathcal{G} , whereas 3 modes are sufficient for the parameter subgroups \mathcal{G}_1 and \mathcal{G}_2 .

We present several tests with 3 different values for L :

- The first situation is with $\Omega = \omega$ (no truncation). Figure 6 depicts the new NIRB error. With the group \mathcal{G} , only 3 and 4 modes are required to retrieve the fine solutions accuracy for $Re = 52$ and $Re = 233$, respectively. With the subgroups \mathcal{G}_1 and \mathcal{G}_2 3 modes are sufficient in both cases. To make the presentation of these results easier, we have first taken $N_1 = N_2$. This test provides more accurate results with the new method (i.e. with (9)) than the classical rectified NIRB (i.e. with (5)) in the case of parameter extrapolation (for example, $Re = 52$ with an RB generated from the subgroup \mathcal{G}_2). In fact, unlike the rectified classical version, the error is almost recovered with $Re = 52$ (with 9 modes).
- Then, we have tested the new algorithm with $L = 3$. We get the same precision as with $\omega = \Omega$ as shown in Figure 7. However, if the new parameter does not belong to the RB subgroup range (\mathcal{G}_1 or \mathcal{G}_2), the error is not recovered with $Re = 52$ and some instabilities are observed.
- Finally, the last tests have been carried out with $L = 1.2$. Because the recirculation area behind the step is cut, this case is much more complex. As a consequence, the results show more instabilities. The importance of λ in the new rectification process (8) is highlighted in this test. Indeed, we compare results obtained with $\lambda = 0$ in Figure 8a to those carried out with $\lambda = 10^{-10}$ in Figure 8b. With this regularization parameter, all the errors remain stable, demonstrating the ability of this new algorithm to retrieve accurate approximations even with highly truncated domains.

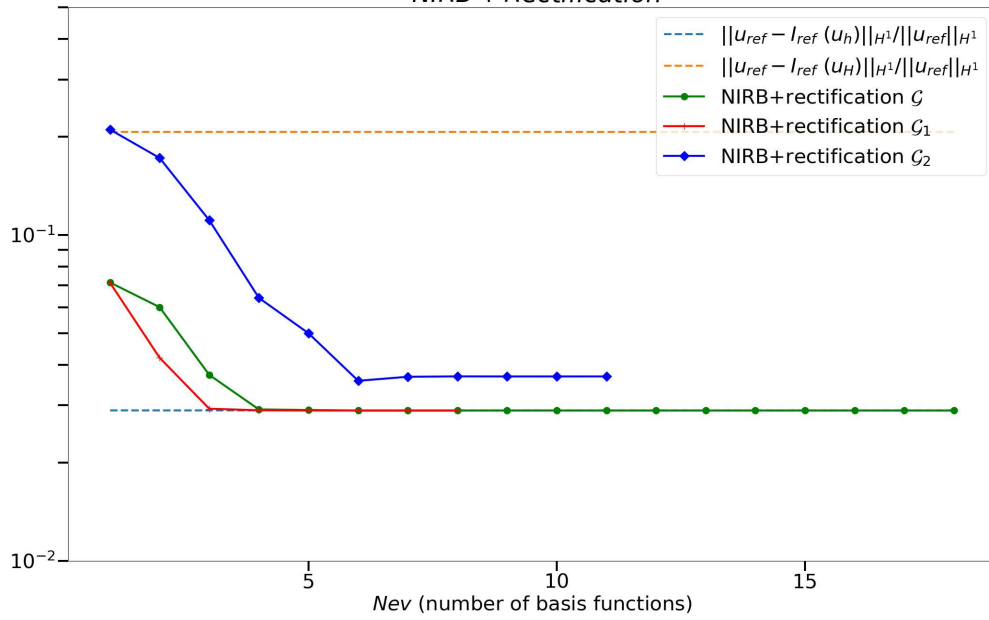
To highlight the influence of N_1 and N_2 , we compare the error between $\mathbf{u}_h(\tilde{\mu})$ and the new NIRB approximation with $L = 1.2$, $L = 3$ and $L = 5$. The errors between the fine solution and the new NIRB approximation are given by

$$\frac{\left\| \mathbf{u}_h(\tilde{\mu}) - \mathbf{T}[\mathbf{u}_{Hh}^N](\tilde{\mu}) \right\|_{H^1(\Omega)}}{\left\| \mathbf{u}_h(\tilde{\mu}) \right\|_{H^1(\Omega)}}. \quad (13)$$

They are presented using heatmaps. Figure 9 presents the results with $\omega = \Omega$. Although there may be some instabilities when the matrix $\mathbf{C}^T \mathbf{C}$ (8) is inverted, as we can see with $N_2 = 18$ with $\lambda = 0$, the error reaches a

Relative errors in H^1 norm with NIRB

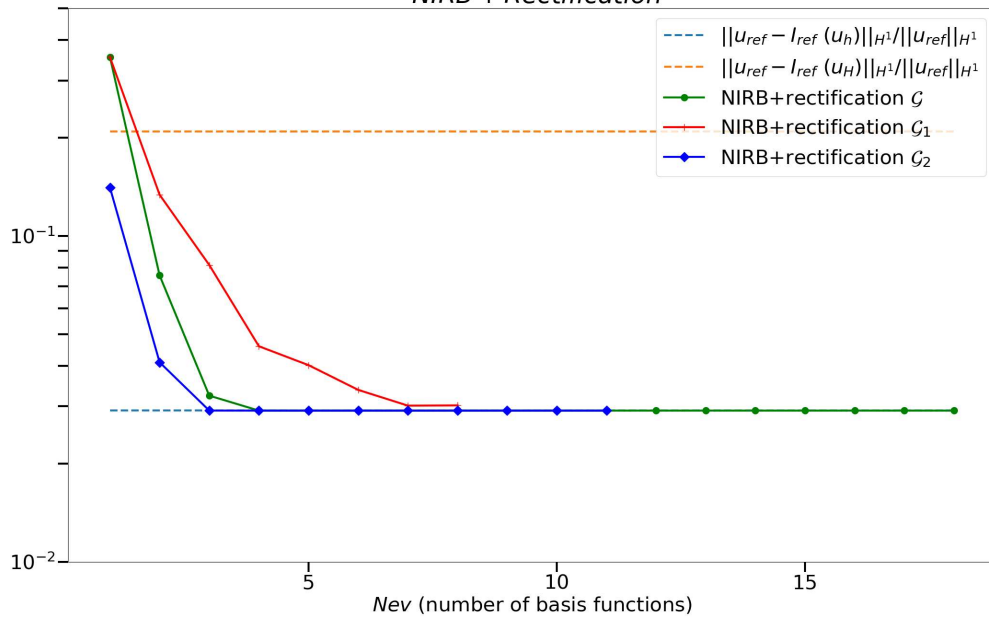
NIRB + Rectification



(a) $Re = 52$

Relative errors in H^1 norm with NIRB

NIRB + Rectification



(b) $Re = 233$

Figure 5: classical NIRB errors with the rectification postprocessing step

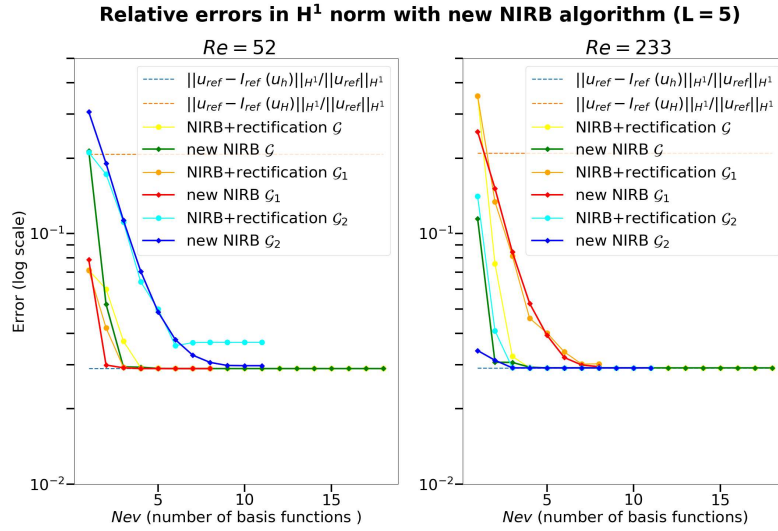


Figure 6: FEM vs NIRB errors: between the reference solution and the NIRB approximations (classical algorithm with rectification vs new NIRB algorithm with $\omega = \Omega$) compared to FEM projection errors (dotted lines), tests with the new parameters $Re = 52$ (left) and $Re = 233$ (right) ($\lambda = 0$).

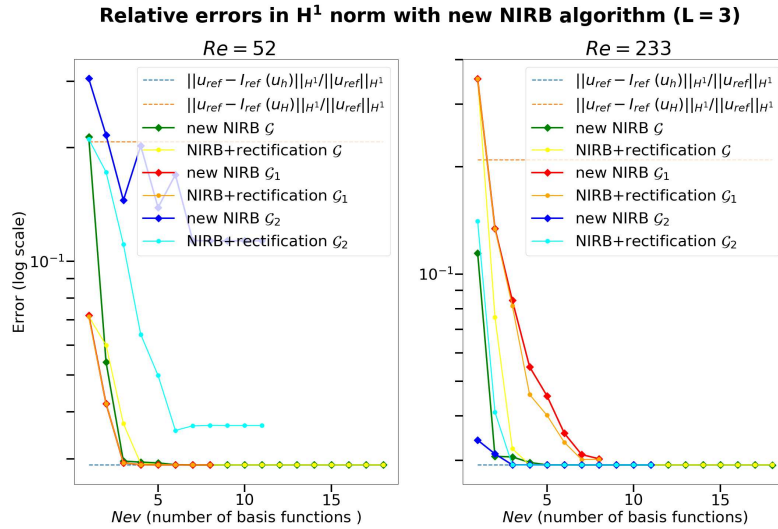
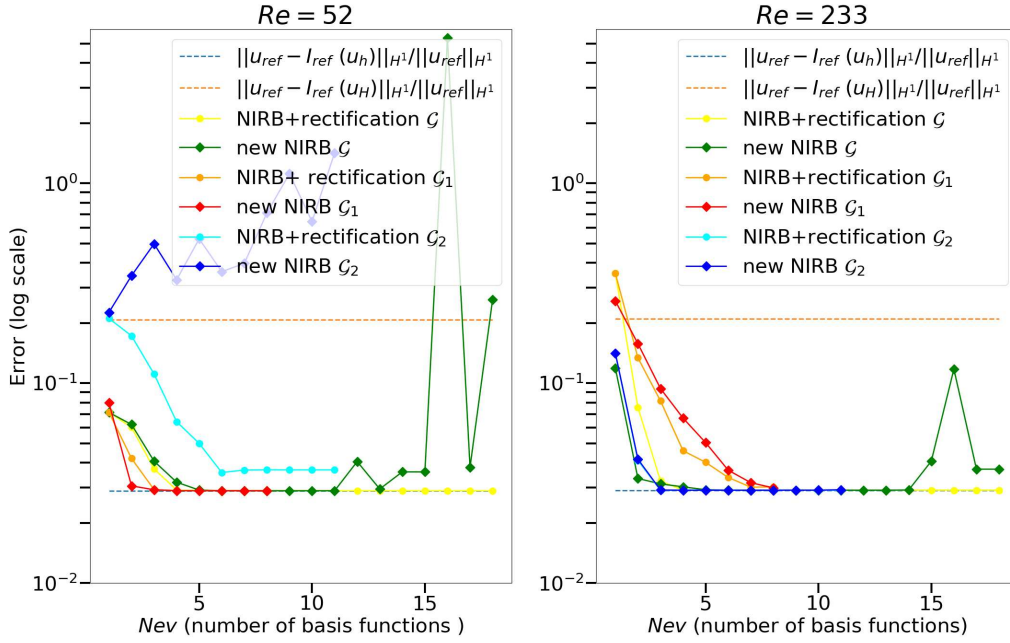


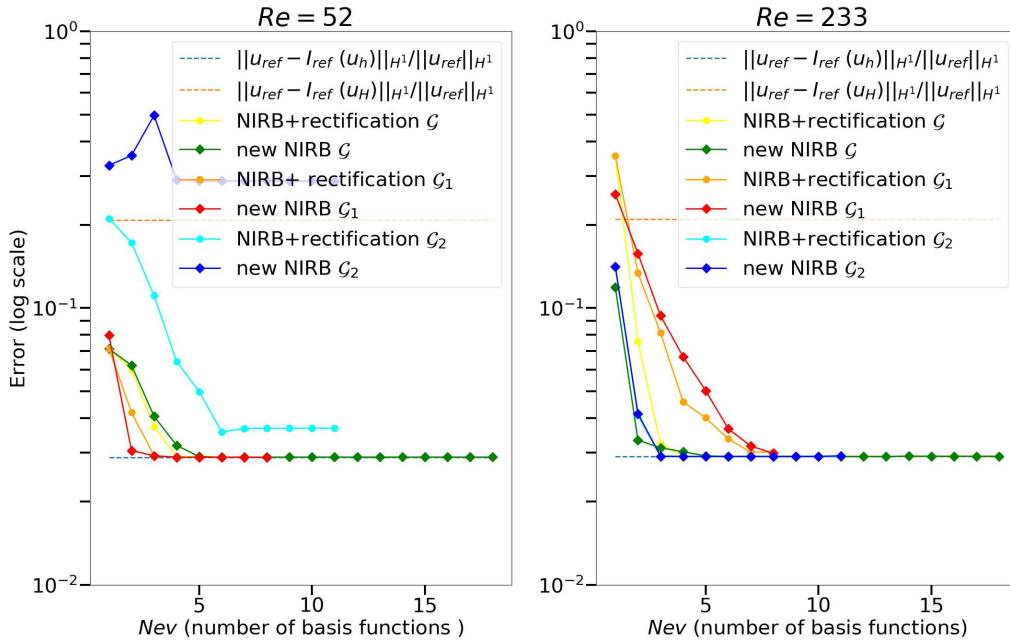
Figure 7: FEM vs NIRB errors: between the reference solution and the NIRB approximations (classical algorithm with rectification vs new NIRB algorithm with $\omega \subset \Omega$) with $L = 3$ compared to FEM projection errors (dotted lines), tests with the new parameters $Re = 52$ (left) and $Re = 233$ (right) ($\lambda = 0$).

Relative errors in H^1 norm with new NIRB algorithm ($L = 1.2$)



(a) $\lambda = 0$

Relative errors in H^1 norm with new NIRB algorithm ($L = 1.2$)



(b) $\lambda = 10^{-10}$

Figure 8: FEM vs NIRB errors: between the reference solution and the NIRB approximations (classical algorithm with rectification vs new NIRB algorithm with $\omega \subset \Omega$) with $L = 1.2$ compared to FEM projection errors (dotted lines), tests with $\lambda = 0$ (left) and $\lambda = 10^{-10}$ (right).

lower threshold than with the classical rectified NIRB approximation. As shown in Figure 10, the term λ set to 10^{-10} allows us to stabilize the errors. We remark in Figure 11 that with $L = 3$, the errors (13) remain smaller than the obtained from the classical NIRB with rectification, with both Reynolds and still quite low when $L = 1.2$ (Figure 12 and Figure 13). Table 1 shows its great ability to reduce computational times.

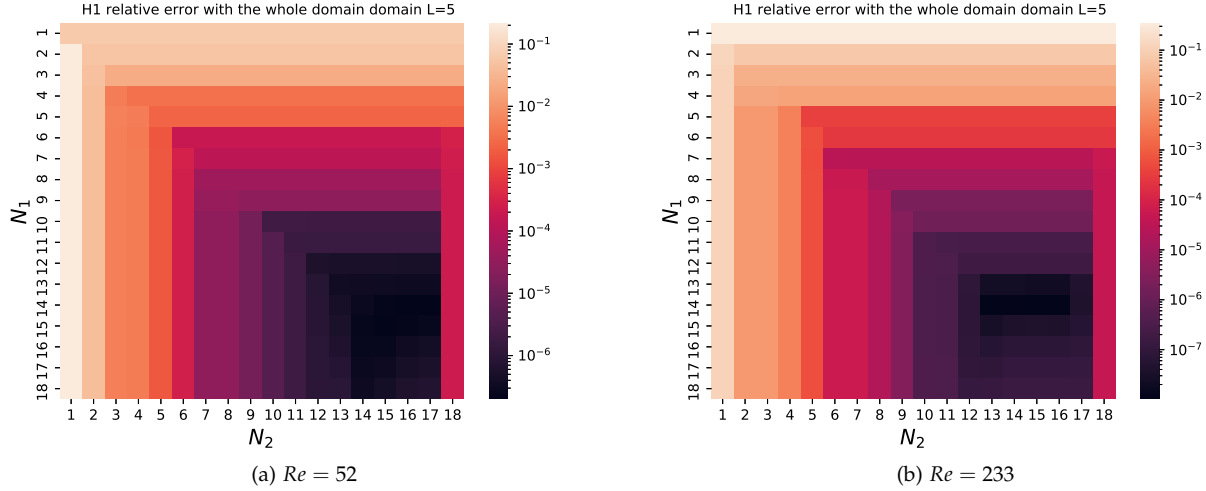


Figure 9: Error of the new NIRB algorithm with $\omega = \Omega$ (no truncation, $L = 5$)

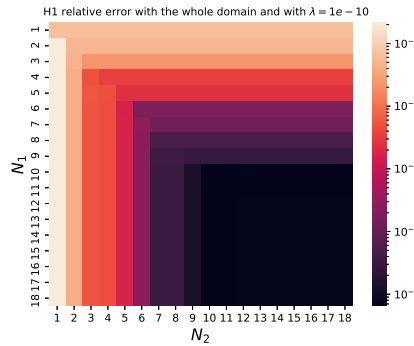


Figure 10: NIRB relative H^1 errors with the new algorithm $\omega = \Omega$ ($L = 5$), $\lambda = 10^{-10}$, $Re = 52$.

We end this section with the new NIRB errors (for u_1 and u_2) and the new NIRB approximations with $L = 3$ and $Re = 52$, $N_1 = 7$, $N_2 = 8$ (Figure 14).

We present the FEM and NIRB runtimes in table 1.

3 NIRB with domain singularities

3.1 Adaptation of the new method to the problem

There are numerous studies on the behaviour of the solutions to elliptic PDE's in domain with re-entrant corners and domain singularities in the literature [7, 4, 46, 45, 31, 29, 13, 20]. The solution lacks regularity and thus, classical uniform regular triangulations do not allow for an approximation with the optimal rate of convergence.

In the case of our numerical analysis in the previous section, because the channel has one re-entrant corner in the BFS problem, it generates a local singularity on the FEM solution. It implies that the latter does not globally lie in $H^2(\Omega)$. In fact, the solution belongs to $H^{1.54448}(\Omega)$ (see, e.g. [3]). Thus, a standard FEM yields reduced

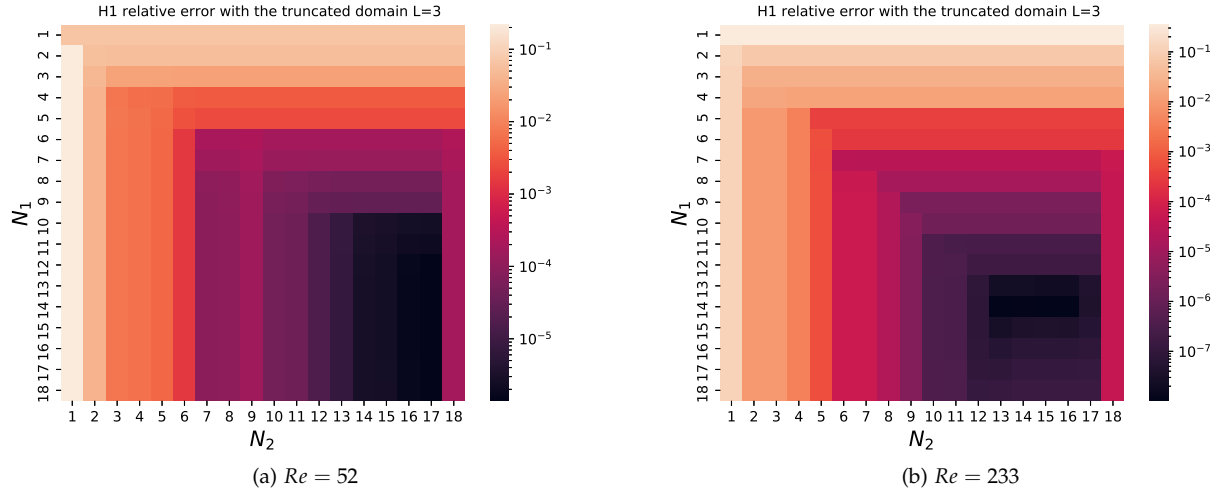


Figure 11: Error of the new NIRB algorithm with $\omega \subset \Omega$, $\lambda = 0$ and \mathcal{G} : $L = 3$

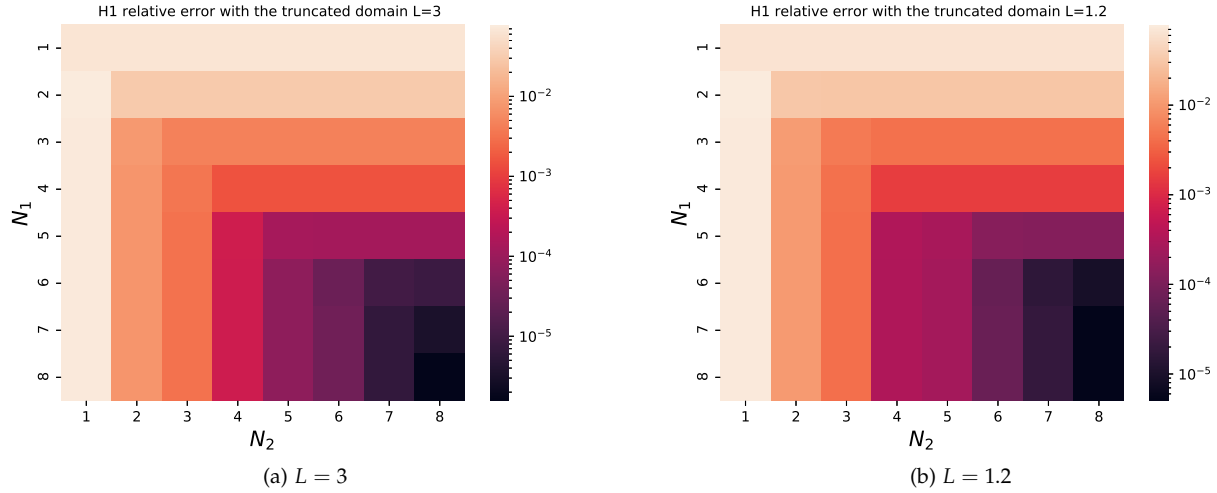


Figure 12: Error of the new NIRB algorithm for the new Reynolds number $Re = 52$ with \mathcal{G}_1 : $L = 3$ and $\lambda = 0$ (left) and with $L = 1.2$ and $\lambda = 10^{-10}$ (right)

Table 1: FEM runtimes min:sec

	FEM high fidelity solver	FEM coarse solution
	00:43	00:01
	NIRB Offline ($N = 18$)	classical NIRB online
	14:30	00:10
	new NIRB offline ($N_1 = N_2 = 18$)	new NIRB online
$\omega = \Omega$	14:52	00:10
$L = 3$	14:52	00:09
$L = 1.2$	14:50	00:09

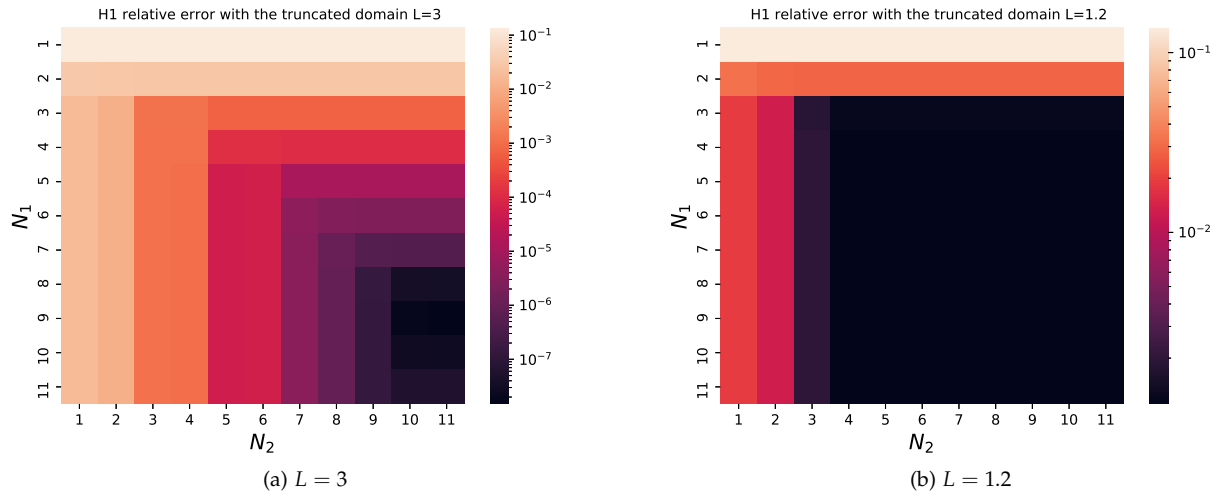


Figure 13: Error of the new NIRB algorithm for the new Reynolds number $Re = 233$ with \mathcal{G}_2 : $L = 3$ and $\lambda = 0$ (left) and with $L = 1.2$ and $\lambda = 10^{-10}$ (right)

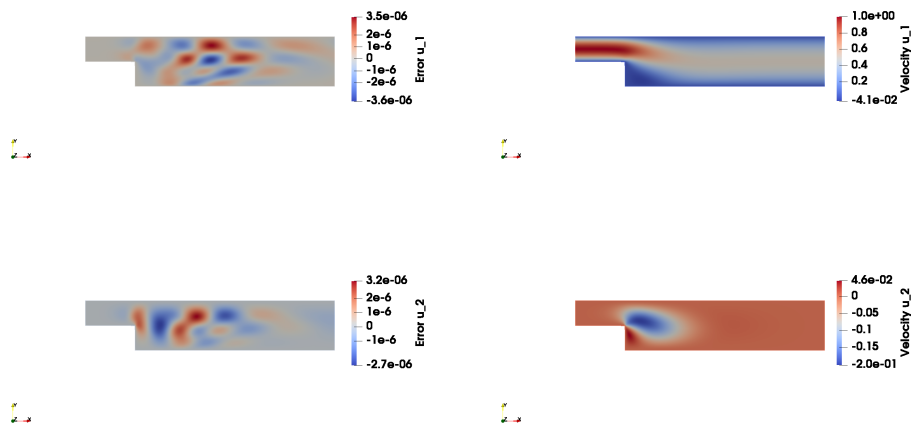


Figure 14: $N_1 = 7$ and $N_2 = 8$, $L = 3$, $Re = 52$ new NIRB error (left) and approximation (right)

convergence rates and the following estimates hold for any $\mu \in \mathcal{G}$ with an uniform mesh of size h :

$$\begin{cases} \|\mathbf{u}(\mu) - \mathbf{u}_h(\mu)\|_{H^1(\Omega)} \leq Ch^{0.54448} \|f\|_{L^2(\Omega)}, \\ \|\mathbf{u}(\mu) - \mathbf{u}_h(\mu)\|_{L^2(\Omega)} \leq Ch^{1.08896} \|f\|_{L^2(\Omega)}, \end{cases}$$

as observed in Figure 15 with the H^1 semi-norm and the L^2 error between the reference and the coarse meshes with the Reynolds number $Re = 52$.

To better approach the solution of such problems and compensate the effects of singularities, most methods rely on adaptive refinements in the vicinity of the singularities, which complicates the resolution of the discrete system, which may not be desirable in the online phase of a NIRB method.

We propose here to follow the same paradigm as in the previous section based on the fair representation of the coarse approximation in terms of its coefficients in a reduced basis that, by a learning approach, allows to retrieve a fine and accurate solution.

The strategy is thus to build, in the first “offline” stage of the NIRB method, an accurate reduced basis relying on an adapted mesh, to correctly capture the singularity and the recirculation zone near the domain reentrant corner. Other methods can also be used. For instance, we may supplement the classical FE basis with singular functions (xFEM) [17, 39]. Another approach employs boundary element methods [29]. We have used an adaptive mesh refinement strategy because they are widely used [1, 4]. They may be based on a-posteriori error estimates [6, 43, 14].

Then we use a coarse uniform mesh “online” to compute an approximate solution (that suffers from the above lack of optimal convergence) that is transformed in a reduced basis representation.

We summarize the offline/online strategy:

1. During the “**offline**” stage, the fine mesh is refined around the re-entrant corners in order to obtain accurate results. Then the offline part of the classical NIRB two-grid with rectification (section 1.1) or its new version with two RB and an appropriate domain truncation (section 2) is applied with this mesh.
2. Then, during the “**online**” part, the coarse approximation is computed on a uniform coarse mesh, and projected and rectified onto the reduced space X_h^N .

3.2 Numerical results

To summarize, in our tests (10), we have employed three meshes:

- a uniform coarse mesh for the coarse FEM approximation,
- a fine mesh refined around the re-entrant corner for the fine snapshots generation,
- and a highly refined mesh for the reference solution to represent the exact solution.

These refinements have been done in FreeFem++ with the “adaptmesh” function. It uses a variable metric/De-launay automatic meshing algorithm [25, 26] (bamg software). With the refinement, the fine mesh size is now defined as

$$h = \min_{K \in \mathcal{M}_h} h_K,$$

where the diameter h_K of any element K in a mesh is equal to $\sup_{x,y \in K} |x - y|$, $K \in \mathcal{T}_h$. With this definition, the reference mesh size is equal to 2.54×10^{-5} .

We have generated $N_1 = N_2 = N = 6$ snapshots ($Re = 5 + 20i$, $i = 0, \dots, 5$) and have tested the new algorithm detailed in section 2 with the truncation parameter $L = 3$ ($\omega \subset \Omega$).

We have experimented four fine meshes with a refinement in the vicinity of the re-entrant corner, as in Figure 17a. We have then used a uniform coarse mesh of size $H \simeq 0.32$ and then an even coarser uniform coarse mesh of size $H \simeq 0.70$ as in Figure 16a. We compare in table 2 the classical NIRB approximation (with the

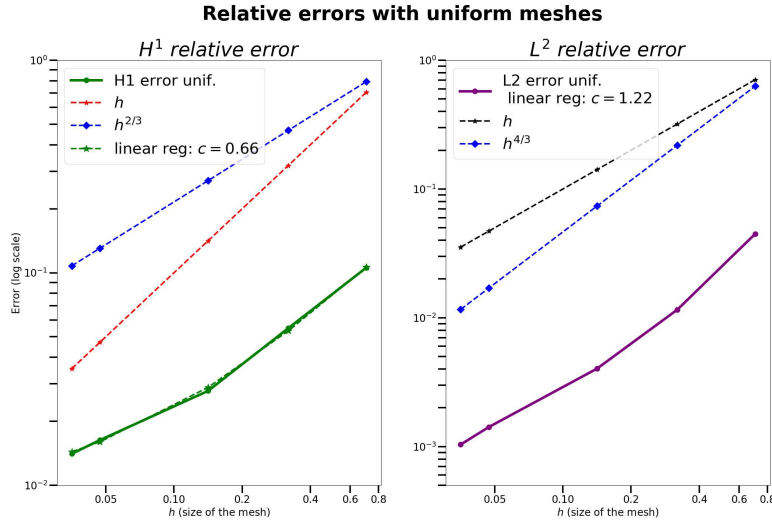


Figure 15: Display of the convergence in H^1 (left) and L^2 (right) of the discrete solution error computed on different uniform grids

rectification post-treatment) with the new approach ($\Omega = \omega$ and $\omega \subset \Omega$). The three NIRB methods recover the fine (refined) mesh accuracy (note that the original NIRB method benefits from the rectification step, indeed, without it, the inaccuracy resulting from the use of a coarse uniform mesh would prevent to recover the fine accuracy).

Table 2: relative errors with the semi H^1 -norm, refined meshes $N_1 = N_2 = N = 6$ with $\lambda = 0$

h	FEM with the fine refined mesh	NIRB with $H = 0.320156$			NIRB with $H = 0.707107$		
		NIRB + Rectification	New NIRB $\omega = \Omega$	New NIRB with $L = 3$ ($\omega \subset \Omega$)	NIRB + Rectification	New NIRB $\omega = \Omega$	New NIRB with $L = 3$ ($\omega \subset \Omega$)
$1.99E^{-4}$	$1.93E^{-3}$	$1.93E^{-3}$	$1.93E^{-3}$	$1.93E^{-3}$	$1.93E^{-3}$	$1.93E^{-3}$	$1.95E^{-3}$
$1.79E^{-4}$	$1.70E^{-3}$	$1.71E^{-3}$	$1.71E^{-3}$	$1.71E^{-3}$	$1.71E^{-3}$	$1.71E^{-4}$	$1.73E^{-3}$
$1.02E^{-4}$	$9.72E^{-4}$	$9.73E^{-4}$	$9.73E^{-4}$	$9.74E^{-4}$	$9.74E^{-4}$	$9.74E^{-4}$	$9.81E^{-4}$
$5.09E^{-5}$	$5.39E^{-4}$	$5.42E^{-4}$	$5.42E^{-4}$	$5.42E^{-4}$	$5.43E^{-4}$	$5.42E^{-4}$	$5.42E^{-4}$

These results are thus promising and illustrate the relevance of this approach.

3.2.1 Time execution (min,sec)

We present the FEM and NIRB runtimes with the meshes as in table 16 for the fine mesh and table 17 for the coarse one, in table 3.

Table 3: FEM runtimes min:sec

FEM HF solver	FEM coarse solution $H = 0.32$
01:24	00:01
NIRB Offline ($N = 6$)	NIRB online
08:34	00:16

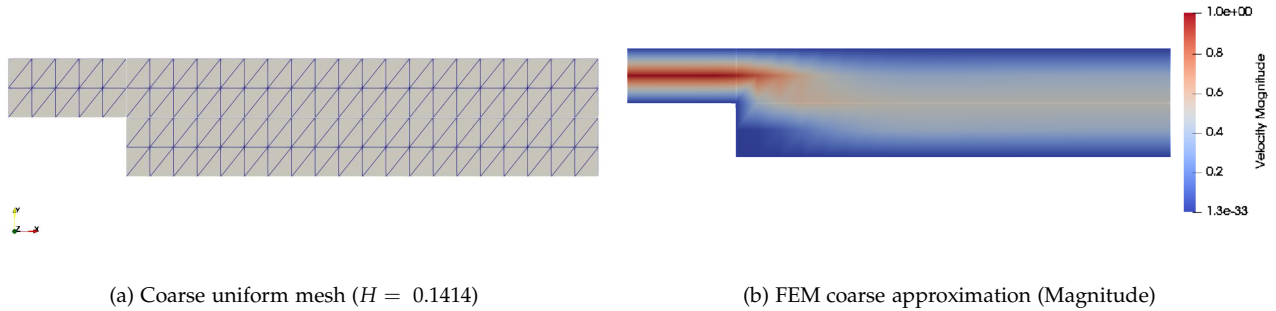


Figure 16: FEM coarse mesh and solution

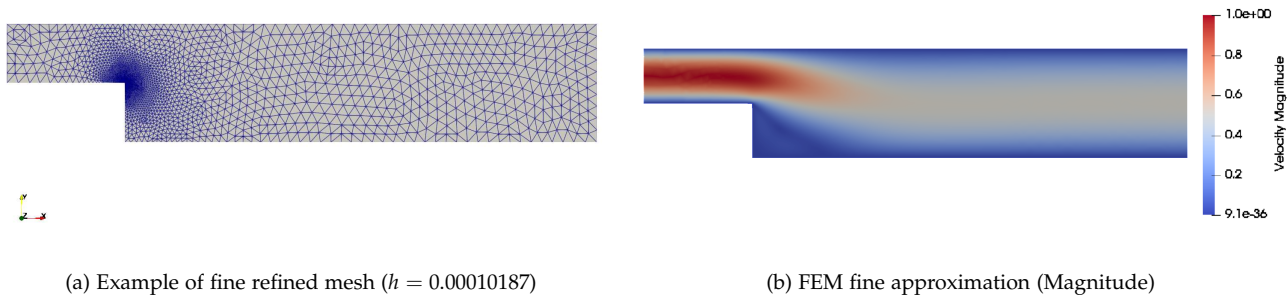


Figure 17: FEM fine mesh and solution

4 Conclusion

We have presented in this paper a new NIRB approach based

- on the construction of two reduced basis: one from some fine and accurate approximation of the solution manifold and one from a coarse approximation,
- and on a truncation of the spatial domain for the coarse approximation.

This new method allows us to use a much coarser mesh during the online stage of the two-grid algorithm, compared to the original method. Indeed, the truncation of the coarse mesh allows to further reduce its complexity. This is what makes this approach so efficient in time. Yet, its size and the domain truncations must be physically acceptable so that there still exist a bijection between the coarse approximations and the associated fine and accurate ones. From the reduced basis coarse components we recover the components of the solution in the fine reduced basis through a deterministic processing stage.

We have applied this new process to the well-known 2D BFS, and obtained the same accuracy than the one given by the fine solutions, while using several truncations.

In the original NIRB two-grid algorithm, the coarse solution needs to be interpolated onto the fine mesh in order to compute the L^2 -projection onto the reduced space X_h^N . Note that the interpolating matrix can be computed during the offline stage but is nevertheless complex. Here with this new algorithm, no interpolation is needed, and in particular, the L^2 -inner product between the coarse solution and the coarse RB is performed on the coarse mesh only.

We even closely consider the effect of the HF simulation involving a mesh refinement to further deal with the singularity of the BFS domain (section 3.1). We numerically show that both the NIRB approaches (original NIRB with rectification and the new tool) allow us to recover the fine FEM accuracy, despite the fact that the coarse approximation is using a uniform (coarse) mesh as observed in table 3.

We believe that this new method may be successfully applied to a wide variety of problems, with complex domains having large number of degrees of freedom, and therefore the computational times will be significantly reduced with a truncated domain.

Acknowledgments

This research was partially funded by the French Fonds Unique Interministeriel (MOR_DICUS).

References

- [1] A. Abdulle and Y. Bai. Reduced basis finite element heterogeneous multiscale method for high-order discretizations of elliptic homogenization problems. *Journal of Computational Physics*, 231(21):7014–7036, 2012.
- [2] M. Barrault, C. Nguyen, A. Patera, and Y. Maday. An ‘empirical interpolation’ method: application to efficient reduced-basis discretization of partial differential equations. *Comptes rendus de l’Académie des sciences. Série I, Mathématique*, 339-9:667–672, 2004.
- [3] C Bernardi and G Raugel. Méthodes d’éléments finis mixtes pour les équations de stokes et de navier-stokes dans un polygone non convexe. *Calcolo*, 18:255–291, 1981.
- [4] S. Brenner. Multigrid methods and stress intensity factors i: Corner singularities. *Mathematics of Computation*, 68(165):559–583, 1999.
- [5] A. Buffa, Y. Maday, A. T. Patera, C. Prud’homme, and G. Turinici. A priori convergence of the greedy algorithm for the parametrized reduced basis method. *ESAIM: Mathematical Modelling and Numerical Analysis-Modélisation Mathématique et Analyse Numérique*, 46(3):595 – 603, 2012.
- [6] P. Burda, J. Novotný, and B. Sousedík. A posteriori error estimates applied to flow in a channel with corners. *Mathematics and Computers in Simulation*, 61(3-6):375–383, 2003.
- [7] A. Carpinteri. Stress-singularity and generalized fracture toughness at the vertex of re-entrant corners. *Engineering Fracture Mechanics*, 26(1):143–155, 1987.
- [8] F. Casenave, A. Ern, and T. Lelièvre. A nonintrusive reduced basis method applied to aeroacoustic simulations. *Advances in Computational Mathematics*, 41(5):961–986, Jun 2014.
- [9] R. Chakir. *Contribution à l’analyse numérique de quelques problèmes en chimie quantique et mécanique*. PhD thesis, 2009. Doctoral dissertation, Université Pierre et Marie Curie-Paris VI.
- [10] R. Chakir and J K. Hammond. A non-intrusive reduced basis method for elastoplasticity problems in geotechnics. *Journal of Computational and Applied Mathematics*, 337:1–17, 2018.
- [11] R. Chakir and Y. Maday. A two-grid finite-element/reduced basis scheme for the approximation of the solution of parametric dependent p.d.e. In *9e Colloque national en calcul des structures*, 2009.
- [12] R. Chakir, Y. Maday, and P. Parnaudeau. A non-intrusive reduced basis approach for parametrized heat transfer problems. *Journal of Computational Physics*, 376:pp.617–633, January 2019.
- [13] Monique Dauge. *Elliptic boundary value problems on corner domains: smoothness and asymptotics of solutions*, volume 1341. Springer, 2006.
- [14] J.P. De SR Gago, D. W. Kelly, O. C. Zienkiewicz, and I. Babuska. A posteriori error analysis and adaptive processes in the finite element method: Part ii—adaptive mesh refinement. *International journal for numerical methods in engineering*, 19(11):1621–1656, 1983.
- [15] F. Durst and C. Tropea. Flows over two-dimensional backward—facing steps. In *Structure of Complex Turbulent Shear Flow*, pages 41–52. Springer, 1983.
- [16] E. Erturk. Numerical solutions of 2-d steady incompressible flow over a backward-facing step, part i: High reynolds number solutions. *Computers & Fluids*, 37(6):633–655, 2008.

- [17] L. C. Foucard and F. J. Vernerey. An x -fem-based numerical–asymptotic expansion for simulating a stokes flow near a sharp corner. *International Journal for Numerical Methods in Engineering*, 102(2):79–98, 2015.
- [18] Rudy Geelen, Stephen Wright, and Karen Willcox. Operator inference for non-intrusive model reduction with quadratic manifolds. *Computer Methods in Applied Mechanics and Engineering*, 403:115717, 2023.
- [19] P. M. Gresho, D. K. Gartling, J.R. Torczynski, K.A. Cliffe, KH Winters, TJ Garratt, A. Spence, and J. W. Goodrich. Is the steady viscous incompressible two-dimensional flow over a backward-facing step at $re=800$ stable? *International Journal for Numerical Methods in Fluids*, 17(6):501–541, 1993.
- [20] Pierre Grisvard. *Elliptic problems in nonsmooth domains*. SIAM, 2011.
- [21] E. Grosjean. *Variations and further developments on the Non-Intrusive Reduced Basis two-grid method*. PhD thesis, 2022. Sorbonne université.
- [22] E. Grosjean and Y. Maday. Error estimate of the non-intrusive reduced basis method with finite volume schemes. *ESAIM: M2AN*, 55(5):1941–1961, 2021.
- [23] E. Grosjean and Y. Maday. Error estimate of the non-intrusive reduced basis (nirb) two-grid method with parabolic equations. *arXiv preprint arXiv:2211.08897*, 2022.
- [24] Mengwu Guo, Shane A McQuarrie, and Karen E Willcox. Bayesian operator inference for data-driven reduced-order modeling. *Computer Methods in Applied Mechanics and Engineering*, 402:115336, 2022.
- [25] F. Hecht. Bamg: bidimensional anisotropic mesh generator. *User Guide. INRIA, Rocquencourt*, 17, 1998.
- [26] F. Hecht. New development in freefem++. *Journal of numerical mathematics*, 20(3-4):251–266, 2012.
- [27] J. S. Hesthaven, G. Rozza, and B. Stamm. *Certified reduced basis methods for parametrized partial differential equations*. Springer, 2016.
- [28] M. A. Hossain, Md. T. Rahman, and S. Ridwan. Numerical investigation of fluid flow through a 2d backward facing step channel. *International Journal of Engineering Research & Technology*, 2(10):3700–3708, 2013.
- [29] H. Igarashi and T. Honma. A boundary element method for potential fields with corner singularities. *Applied Mathematical Modelling*, 20(11):847–852, 1996.
- [30] O. Iliev, Y. Maday, and T. Nagapetyan. *A Two-grid Infinite-volume/reduced Basis Scheme for the Approximation of the Solution of Parameter Dependent PDE with Applications the AFFFF Devices*. Fraunhofer Inst. für Techno-und Wirtschaftsmathematik, ITWM. Citeseer, 2013.
- [31] S. Kim and H-C. Lee. A finite element method for computing accurate solutions for poisson equations with corner singularities using the stress intensity factor. *Computers and Mathematics with Applications*, 71(11):2330–2337, 2016. Proceedings of the conference on Advances in Scientific Computing and Applied Mathematics. A special issue in honor of Max Gunzburger’s 70th birthday.
- [32] A. Kolmogoroff. Über die beste annäherung von funktionen einer gegebenen funktionenklasse. *Annals of Mathematics*, pages 107–110, 1936.
- [33] T. Lee and D. Mateescu. Experimental and numerical investigation of 2-d backward-facing step flow. *Journal of Fluids and Structures*, 12(6):703–716, 1998.
- [34] Zhendong Luo, Juan Du, Zhenghui Xie, and Yan Guo. A reduced stabilized mixed finite element formulation based on proper orthogonal decomposition for the non-stationary navier–stokes equations. *International Journal for Numerical Methods in Engineering*, 88(1):31–46, 2011.
- [35] Andrea Manzoni. An efficient computational framework for reduced basis approximation and a posteriori error estimation of parametrized navier–stokes flows. *ESAIM: Mathematical Modelling and Numerical Analysis*, 48(4):1199–1226, 2014.
- [36] Thomas O’Leary-Roseberry, Xiaosong Du, Anirban Chaudhuri, Joaquim RRA Martins, Karen Willcox, and Omar Ghattas. Learning high-dimensional parametric maps via reduced basis adaptive residual networks. *Computer Methods in Applied Mechanics and Engineering*, 402:115730, 2022.

- [37] D. B. Phuong Huynh, D. J. Knezevic, and A. T. Patera. A static condensation reduced basis element method : approximation and a posteriori error estimation. *ESAIM: M2AN*, 47(1):213–251, 2013.
- [38] A. Quarteroni, A. Manzoni, and F. Negri. *Reduced Basis Methods for Partial Differential Equations: an introduction*, volume 92. Springer, 2015.
- [39] D. Rabinovich, D. Givoli, and S. Vigdergauz. Xfem-based crack detection scheme using a genetic algorithm. *International Journal for Numerical Methods in Engineering*, 71(9):1051–1080, 2007.
- [40] G. Stabile, S. Hijazi, A. Mola, S. Lorenzi, and G. Rozza. Pod-galerkin reduced order methods for cfd using finite volume discretisation: vortex shedding around a circular cylinder. *Communications in Applied and Industrial Mathematics*, 8(1):210–236, 2017.
- [41] A. N. Tikhonov. Solution of incorrectly formulated problems and the regularization method. *Soviet Math. Dokl.*, 4:1035–1038, 1963.
- [42] Sebastian Ullmann, Marko Rotkvic, and Jens Lang. Pod-galerkin reduced-order modeling with adaptive finite element snapshots. *Journal of Computational Physics*, 325:244–258, 2016.
- [43] R. Verfürth. A posteriori error estimation and adaptive mesh-refinement techniques. *Journal of Computational and Applied Mathematics*, 50(1-3):67–83, 1994.
- [44] K. Veroy, C. Prud’Homme, and A. T. Patera. Reduced-basis approximation of the viscous Burgers equation: rigorous a posteriori error bounds. *Comptes rendus de l’Académie des sciences. Série I, Mathématique*, 337(9):619–624, November 2003.
- [45] L. B. Wahlbin. On the sharpness of certain local estimates for H^1 projections into finite element spaces: Influence of a reentrant corner. *Mathematics of Computation*, 42(165):1–8, 1984.
- [46] L. B. Wahlbin. Local behavior in finite element methods. In *Finite Element Methods (Part 1)*, volume 2 of *Handbook of Numerical Analysis*, pages 353–522. Elsevier, 1991.